High-frequency gravitational waves having large spectral densities and their electromagnetic response*

Li Fang-Yu(李芳昱)†, Wen Hao(文 毫), and Fang Zhen-Yun(方祯云)

Department of Physics, Chongqing University, Chongqing 400044, *China*

(Received 9 April 2013; revised manuscript received 20 May 2013)

Various cosmology models, brane oscillation scenarios, interaction of interstellar plasma with intense electromagnetic radiation, and even high-energy physics experiments (e.g., Large Hadron Collider (LHC)) all predict high frequency gravitational waves (HFGWs, i.e., high-energy gravitons) in the microwave band and higher frequency region, and some of them have large energy densities. Electromagnetic (EM) detection to such HFGWs would be suitable due to very high frequencies and large energy densities of the HFGWs. We review several typical EM detection schemes, i.e., inverse Gertsenshtein effect (G-effect), coupling of the inverse G effect with a coherent EM wave, coupling of planar superconducting open cavity with a static magnetic field, cylindrical superconducting closed cavity, and the EM sychro-resonance system, and discuss related minimal detectable amplitudes and sensitivities. Furthermore, we give some new ideas and improvement ways enhancing the possibility of measuring the HFGWs. It is shown that there is still a large room for improvement for those schemes to approach and even reach up the requirement of detection of HFGWs expected by the cosmological models and high-energy astrophysical process.

Keywords: high-frequency gravitational waves, electromagnetic response of high-frequency gravitational waves, superconducting microwave cavities, synchro-resonance system

PACS: 04.30.Nk, 04.25.Nx, 04.30.Db, 04.80.Nn **DOI:** 10.1088/1674-1056/22/12/120402

1. Introduction

In recent years, the research on high frequency gravitational waves (HFGWs) attract more interest and attention.[1–6] Frequencies of these HFGWs are often higher or much higher than 10^5 Hz (According to definition of HFGWs by Press and Thorne,[7] the HFGWs are GWs whose frequencies excess 10^5 Hz).The main reasons are as follows:

(i) The peak region and partial peak region of energy densities expected by a series of typical contemporary cosmological models such as the pre-big-bang model,[8–10] the quintessential inflationary models,[3,4] the ekpyrotic models[10] are just localized in the GHz band, and the upper limit of the energy densities might reach up to $\Omega_{\rm gw} \sim 6.9 \times 10^{-6}$. This means that the corresponding upper limit of dimensionless amplitudes of the relic HFGWs in the GHz band would be $h \sim 10^{-30}$ to 10^{-31}.

(ii) The upper limit of dimensionless amplitudes of HFGWs in brane oscillation scenarios[11] would be expected to be $\sim 10^{-22}$ in the earth region in the GHz to the THz band. This means that the upper limit of energy densities of such HFGWs in brane oscillation scenarios are obviously higher than that in the relic HFGWs.

(iii) Interaction of astrophysical plasma with intense electromagnetic waves[5,12] could generate HFGWs in the microwave band even higher frequency ranges. Moreover, some thermal GW models and a possible new physical mechanism[13] also predict the HFGWs in a broad high-frequency region, and dimensionless amplitudes expected by them are from a very small value $h \sim 10^{-40}$ to the upper limit $h \sim 10^{-24}$.

(iv) Some high-energy physics experiments might generate HFGWs and very high frequency HFGWs,[14–18] but their dimensionless amplitudes are often very small values ($h \sim 10^{-39}$ to 10^{-41}). However, the frequencies of these HFGWs may be extended into a very high range ($\nu_{\rm g} \sim 10^{21}$ Hz to 10^{23} Hz), thus the high-energy accelerators, such as the Linear Collider, and the especially constructed Large Hadron Collider (LHC)[15] are possible to produce gravitons having higher energies.

However, unlike usual GW detection in the intermediate-frequency band ($\nu \sim 1$ Hz to 1000 Hz) and in the low-frequency band ($\mu \sim 10^{-7}$ Hz to 1 Hz), where the crucial parameter is the dimensionless amplitude of GW (the signals generated by the GWs in these detectors majorly depend on the amplitudes of GWs and they are almost independent of the frequencies of GWs in their detection frequency bands), in some of the EM detection systems, EM perturbative effects (signal) depend not only on the amplitudes of GWs, but also their frequencies, i.e., a very high frequency would compensate for weak HFGW amplitude, especially the coupling system between the EM microwave beam and the static magnetic filed. In this case, the interaction cross section of HFGW (high-

*Project supported by the National Natural Science Foundation of China (Grant Nos. 11075224 and 11375279) and the Foundation of China Academy of Engineering Physics (Grant Nos. 2008 T0401 and T0402).

†Corresponding author. E-mail: fangyuli@cqu.edu.cn

© 2013 Chinese Physical Society and IOP Publishing Ltd

energy gravitons) with resonant EM wave (photons) in a static magnetic field (virtual photon background) can be much larger than direct interaction of GW (gravitons) with EM wave (photons) or with a static magnetic field (virtual photons). Therefore, considerations and estimations as to the EM perturbation and minimal detectable signal in some of the EM detection systems would be significant for detection of the HFGWs.

Moreover, we shall give a brief review and discussion for the following hot issues: Are there further improvements for the present HFGW detection schemes? Can the sensitivity be effectively improved by the combination of the static magnetic field with a background EM wave beam? If so, what are the key conditions and methods for the improvement of the sensitivity? Why does our synchro-resonance system (SRS) have a lower standard quantum limit? These answers would provide a clear response and possible solution for such issues. In this paper we shall discuss some typical EM detection systems, minimal detectable signals, and possible improvement ways.

This paper includes the following three parts: Section 1 is an Introduction. In Section 2 we review and discuss various typical EM detection systems and their EM response to the HFGW, including: 1) the EM response in system of the inverse Gertsenshtein effect (inverse G-effect). 2) the EM response in the coupling system of the inverse G-effect with a coherent plane EM waves; 3) the EM response in coupling systems of planar open superconducting cavity with a static magnetic field; 4) the EM response in the coupling system of a closed cylindrical superconducting cavity with a static magnetic field; and 5) the EM response in a system of synchro-resonance effect. In this section we also discuss and give some ideas and possible improvement ways for such EM detection systems of measuring these HFGWs. In Section 3 we make concluding remarks.

2. Electromagnetic perturbative effects and minimal detectable signal of the high-frequency gravitational waves (HFGWs)

2.1. EM perturbation in the inverse Gertsenshtein effect

The physical basis of the Gertsenshtein effect (G-effect) is the Einstein–Maxwell equations,[19] i.e., when an EM wave propagates in transverse homogeneous static magnetic fields, it can generate GW (gravitons flux). Contrarily, the physical basis of the inverse G-effect is the electrodynamics in curved spacetime,[20,21] that is, if a GW passes through a transverse homogeneous static magnetic field, then it can produce an EM wave (phono flux). For the inverse G-effect in the laboratory size, the wavelength of GWs should be comparable with the laboratory dimension, in other words, these GWs should be HFGWs in the microwave band ($\sim 10^8$ Hz to 10^{12} Hz).

According to electrodynamical equations in curved spacetime, the EM wave generated by the incoming HFGW with the static magnetic field can be given by[20,22]

$$\begin{aligned}\tilde{E}_x^{(1)} &= \frac{1}{2}A\hat{B}_y^{(0)}k_{\rm g}cL\sin(k_{\rm g}z-\omega_{\rm g}t),\\ \tilde{B}_y^{(1)} &= \frac{1}{2}A\hat{B}_y^{(0)}k_{\rm g}L\sin(k_{\rm g}z-\omega_{\rm g}t),\end{aligned} \tag{1}$$

where A is the amplitude of HFGW, L is the interaction dimension between the HFGW, and $\hat{B}_y^{(0)}$ is the static magnetic field. Here, we neglected the perturbative EM fields propagating along the negative z direction (i.e., the opposite propagating direction from the incoming HFGW), because they are much weaker or absent.[20–22] Equation (1) is actually the maximum of perturbative electromagnetic (EM) fields (in the terminal position of the interaction volume) due to the space accumulation effect in the propagating direction of HFGW. Thus, the EM power flux at the receiving surface Δs of the terminal position is

$$U^{(2)} = \frac{1}{2\mu_0}\,{\rm Re}[\tilde{E}_x^{(1)*}\tilde{B}_y^{(1)}]\Delta s = \frac{1}{8\mu_0}(A\hat{B}_y^{(0)}k_{\rm g}L)^2c\Delta s. \tag{2}$$

Or in a quantum language, perturbative photon flux (PPF), i.e., signal photon flux will be

$$\begin{aligned}n^{(2)} &= \tilde{U}^{(2)}/\hbar\omega_e = \frac{A^2}{8\mu_0\hbar\omega_e}(\hat{B}_y^{(0)}k_{\rm g}L)^2c\Delta s\\ &= \frac{(A\hat{B}_y^{(0)}L)^2\omega_{\rm g}}{8\mu_0c\hbar}\Delta s,\end{aligned} \tag{3}$$

where the superscripts 1 and 2 denote the first-order and second-order perturbations, respectively. Notice that here $n^{(2)} \propto \omega_{\rm g}$, which means that HFGWs (high-energy gravitons) have a larger interaction cross section to the static magnetic field than intermediate- and low-frequency GWs (low-energy gravitons). Because the minimal detectable power flux corresponds to the minimal detectable amplitude of HFGW, from Eq. (2) we have,

$$h_{\rm min} = \sqrt{\frac{8\mu_0U_{\rm min}^{(2)}}{\hat{B}_y^{(0)^2}k_{\rm g}^2L^2c\Delta s}} = \frac{1}{\hat{B}_y^{(0)}\omega_{\rm g}L}\sqrt{\frac{8\mu_0cU_{\rm min}^{(2)}}{\Delta s}}, \tag{4}$$

equation (4) and the result in Ref. [6] are completely self-consistent. In Ref. [6] the minimal detectable signal power is $K\Delta T_{\rm min}$ (K is Boltzmann constant).

Equation (4) shows the following important properties. The first is $h_{\rm min} \propto 1/\omega_{\rm g}$, this means that for the same $U_{\rm min}$, a higher frequency behaves better for a detectable signal. Thus the HFGWs with larger energy densities have a better perturbative effect. The second is $h_{\rm min} \propto 1/\hat{B}^{(0)}L\sqrt{\Delta s}$, this means that in order to generate a detectable signal, a detector based on the inverse G-effect should have a background static magnetic field $B^{(0)}$, the interaction dimension L, and an effective receiving surface Δs (i.e., the interaction volume) as large as possible. Under the current technological condition, the detectable minimal power would be $\sim 10^{-22}$ W in a 1-Hz bandwidth in the microwave band.[6] Then, putting $U_{\rm min} = 10^{-22}$ W,

$B^{(0)} = 9$ T, $\Delta L = 3$ m, $\Delta s = 0.36$ m^2, ($\Delta s = 0.6$ m$\times$0.6 m), then one finds:

$$\begin{aligned} h_{\min} &= 1.8\times10^{-21} \text{ for } \nu_g = 3\times10^9 \text{ Hz}, \\ h_{\min} &= 1.8\times10^{-24} \text{ for } \nu_g = 3\times10^{12} \text{ Hz}. \end{aligned} \tag{5}$$

Notice that the upper limit of the amplitude of the HFGWs in the brane oscillation model would be $h \sim 10^{-22}$ in the earth region in the GHz band to the THz band.[11] Thus, if the brane oscillation model is correct, and the point-like objects orbiting a brane world black hold in our galaxy would be a promising HFGW sources, and the HFGWs in brane oscillation models would be detectable. However, amplitudes of relic HFGWs expected by almost all typical cosmological models[2–4,8–10] would be 10^{-29} to 10^{-30} or less in the GHz band, and considering the stochastic features of relic HFGWs and the movement effect of the earth, a detection scheme based on the pure inverse G-effect could not detect relic HFGWs in the laboratory condition.

2.2. The coupling of the inverse Gertsenshtein effect with a coherent plane electromagnetic wave

If the HFGW and the plane EM wave having the same frequency pass through simultaneously the transverse static magnetic field (i.e., resonance coupling system), then first-order perturbative EM power flux (signal) (see Fig. 1) can be given by[23]

$$\begin{aligned} U^{(1)} &= \frac{1}{2\mu_0}\langle \tilde{\boldsymbol{E}}^{(0)*} \times \tilde{\boldsymbol{B}}_y^{(1)} \rangle_{\omega_e=\omega_g} \Delta s \\ &= \frac{1}{4\mu_0} \mathrm{Re}[\tilde{E}^{(0)*}\tilde{B}_y^{(1)}]_{\omega_e=\omega_g} \sin\beta\cos\delta\Delta s, \end{aligned} \tag{6}$$

where the superscripts 0 and 1 denote the background and first-order perturbative EM fields, respectively, β is the angle between $\tilde{\boldsymbol{E}}^{(0)}$ and $\tilde{\boldsymbol{B}}_y^{(1)}$, and δ is the phase difference of them (it is also the phase difference between the HFGW and the background EM wave). Thus, from Eqs. (1) and (6), the maximum of $U^{(1)}$ is

$$\begin{aligned} U^{(1)}_{\beta=\pi/2,\delta=0} &= U^{(1)}_{\max} = \frac{1}{4\mu_0}\langle \tilde{E}^{(0)*}\tilde{B}_y^{(1)} \rangle_{\omega_e=\omega_g}\Delta s \\ &= \frac{1}{4\mu_0} A\hat{B}_y^{(0)}\tilde{E}^{(0)} k_g L \Delta s, \end{aligned} \tag{7}$$

so the corresponding maximum of the PPF is

$$n^{(1)}_{\max} = U^{(1)}_{\max}/\hbar\omega_e = \frac{1}{4\mu_0\hbar c} A\hat{B}_y^{(0)}\tilde{E}^{(0)} L\Delta s. \tag{8}$$

Because $|A| \ll 1$ for the HFGWs, the signal power flux (first-order EM perturbation) expressed by Eq. (7) is much larger than the second-order EM perturbation presented by Eq. (2).

However, such a larger signal power flux (larger interaction cross section) does not lead to a much better sensitivity. This is because the presence of the background EM power flux (or in quantum language, the background photon flux (BPF)) will generate a large noise photon flux. In the case of a plane EM wave, the first-order PPF (signal photon flux) and the BPF have the same or very similar physical behaviors, including the propagating direction and distribution (see Fig. 1). Then the PPF will be swamped by the noise BPF. In fact, we have already pointed out this property in our previous works (e.g., see Refs. [23] and [24]). Here it should be better to emphasize this feature again.

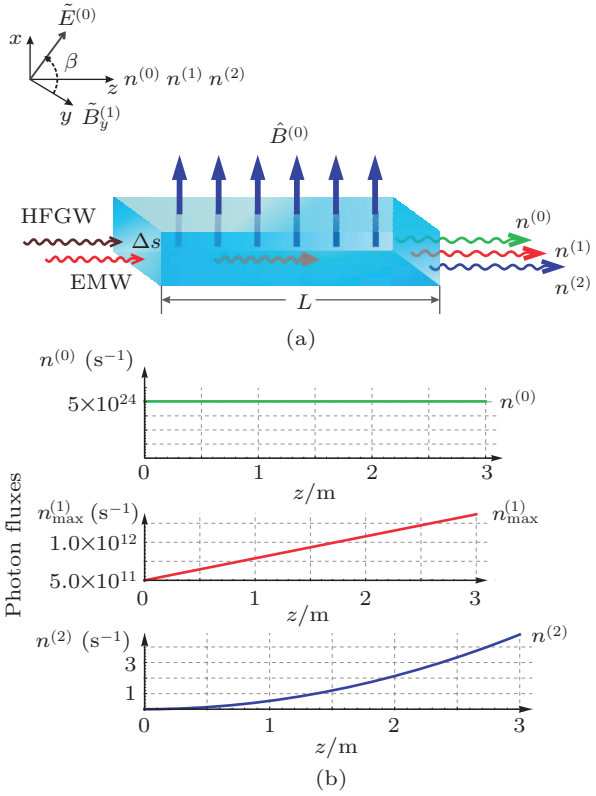


Fig. 1. (color online) (a) The coupling system of the inverse Gertsenshtein effect with a coherent plane electromagnetic wave; (b) Function curves of background photon flux, first-order PPF, and second-order PPF. The panel (a) shows: when the frequency ν_e of the background EM wave and the frequency ν_g of the incoming HFGW are the same and they satisfy the suitable coherent condition, the first-order PPF, $n^{(1)}_{\max}$, and the second-order PPF, $n^{(2)}$ can be generated, and $n^{(1)}_{\max} \gg n^{(2)}$. However, the presence of the background photon flux BPF, $n^{(0)}$, will generate a large noise photon flux. Because $n^{(1)}_{\max}$ and $n^{(0)}$ have the same propagating direction and distribution, and $n^{(1)}_{\max} \ll n^{(0)}$, so $n^{(1)}_{\max}$ will be swamped by $n^{(0)}$, where $n^{(2)}$ is the signal photon flux in the pure inverse Gertsenshtein effect (G-effect), $n^{(1)}_{\max}$ is the maximum of the signal photon flux in the coupling system of the inverse G-effect with the coherent plane EM wave. Notice that $n^{(2)} \propto A^2z^2$ (nonlinear relation), $n^{(1)}_{\max} \propto Az$ (linear relation), and $A \ll 1$. Thus, the sensitivity in the coupling system may be improved by one to two orders of magnitude, but cannot be improved much beyond the pure inverse G-effect. The panel (b) shows the background photon flux $n^{(0)}$, the maximum of the first-order perturbative photon flux $n^{(1)}_{\max}$ and the second-order perturbative photon flux $n^{(2)}$. Here typical parameters are $h = 10^{-21}$, $\nu_g = 3\times10^9$ Hz, $B^{(0)} = 9$ T, $\Delta l = 3$ m, $P = 10$ W (the power of the plane EM wave) and $\Delta s = 0.36$ m^2 (the receiving surface).

It is interesting to compare their ratio of the first-order

PPF, Eq. (8), to the second-order PPF, Eq. (3), that is,

$$\eta = n^{(1)}_{\max}/n^{(2)} = \frac{2\tilde{E}^{(0)}}{A\hat{B}^{(0)}_y k_g Lc}. \tag{9}$$

For the typical parameters: $A = 1.8\times10^{-21}$, $\hat{B}^{(0)}_y = 9$ T, $L = 3$ m, $k_g = 62.8$ ($\nu_e = \nu_g = 3\times10^9$ Hz), $\tilde{E}^{(0)} = 45.8$ V·m^{-1} (for the plane EM wave of $P = 10$ W passing through the receiving surface $\Delta s = 0.36$ m^2), from Eqs. (8) and (9), we find

$$n^{(1)}_{\max} = 5.0\times10^{12}\ \mathrm{s}^{-1},\ \text{and}\ \ \eta = 1.0\times10^{11}. \tag{10}$$

In this case, in order to detect a smaller signal, it is necessary to spend a long enough accumulation time of the signal to distinguish the PPF (signal) from the noise photon flux fluctuation of the BPF. For example, in order to detect the HFGW of $h = 10^{-23}$ and $\nu_g = 3\times10^9$ Hz, $\Delta t_{\min}$ should be 6.4×10^3 s or larger. Thus, the sensitivity in the coupling system of the inverse G-effect with the coherent plane EM wave can be improved one to two orders of magnitude, but it cannot be effectively improved much beyond the pure inverse G-effect.

2.3. Coupling of the planar superconducting open cavity with a static magnetic field

Unlike the EM response to the HFGWs in the free space (e.g., the inverse G effect), the perturbative EM fields in the cavity must satisfy the boundary condition at the cavity walls, and where very small but non-vanishing Ohmic losses correspond to a very large quality factor Q.

Figure 2 shows a coupling system of a planar open cavity with a static magnetic field. If the static magnetic field $\hat{B}^{(0)}$ is a unique non-vanishing background EM field, according to the electrodynamical equations in curved spacetime and the boundary condition at the cavity walls, the perturbative EM normal modes produced by the linear polarized HFGW propagating along the z axis can be given by[25,26]

$$\begin{aligned}
\tilde{E}^{(1)}_x &= \mathrm{i}2A_{\oplus}\hat{B}^{(0)}cQ\sin\left(\frac{n\pi}{b}z\right)\exp[-\mathrm{i}(\omega_g t+\delta)],\\
\tilde{B}^{(1)}_y &= 2A_{\oplus}\hat{B}^{(0)}Q\cos\left(\frac{n\pi}{b}z\right)\exp[-\mathrm{i}(\omega_g t+\delta)],\\
\tilde{E}^{(1)}_y &= -2A_{\otimes}\hat{B}^{(0)}cQ\sin\left(\frac{n\pi}{b}z\right)\exp[-\mathrm{i}(\omega_g t+\delta)],\\
\tilde{B}^{(1)}_x &= -\mathrm{i}2A_{\otimes}\hat{B}^{(0)}Q\cos\left(\frac{n\pi}{b}z\right)\exp[-\mathrm{i}(\omega_g t+\delta)],
\end{aligned} \tag{11}$$

where Q is the quality factor of the open cavity, b is the distance between two parallel cavity walls, n is an integer, and $A_{\oplus}$ and $A_{\otimes}$ are the amplitudes of the $\oplus$-type and $\otimes$-type polarization components of the HFGW, respectively. For the HFGW of $\nu_g = 3\times10^9$ Hz, its wavelength is $\lambda_g = 10$ cm. Under the resonance condition of the fundamental frequency, we have $k_e = k_g = 2\pi/\lambda_g = 2\pi/\lambda_e = \pi/b$ (here $n = 1$ in Eq. (11)), thus $b = \lambda_g/2 = 5$ cm (see Fig. 2).

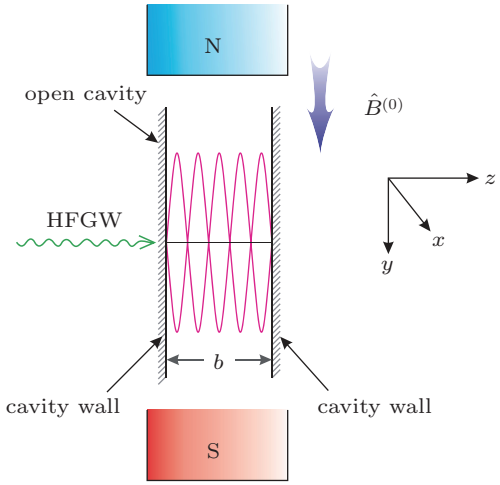


Fig. 2. (color online) Planar open superconducting cavity and coupling EM fields. The coupling system consists of an open superconducting cavity, a static magnetic field pointing along the y axis, where b is the distance between two parallel cavity walls.

From Eq. (11), the total perturbative EM energy in the cavity produced by the HFGW can be given by

$$\begin{aligned}
\mathscr{E}^{(2)} &= \langle \overset{(2)}{T^0_0}\rangle V = \frac{1}{\mu_0}\left\langle -F^{(1)}_{0\alpha}F^{0\alpha(1)} + \frac{1}{4}F^{(1)}_{\alpha\beta}F^{\alpha\beta(1)}\right\rangle V\\
&= \frac{1}{2}\mathrm{Re}\left[\varepsilon_0(\tilde{E}^{(1)*}_x\tilde{E}^{(1)}_x + \tilde{E}^{(1)*}_y\tilde{E}^{(1)}_y)\right.\\
&\quad \left. + \frac{1}{\mu_0}(\tilde{B}^{(1)*}_x\tilde{B}^{(1)}_x + \tilde{B}^{(1)*}_y\tilde{B}^{(1)}_y)\right]V\\
&= \frac{2}{\mu_0}(\hat{B}^{(0)}Q)^2(A^2_{\oplus}+A^2_{\otimes})V,
\end{aligned} \tag{12}$$

where $\overset{(2)}{T^0_0}$ is the 0–0 component of the second-order perturbation of the energy–momentum tensor of the EM fields in the HFGW, $F^{(1)}_{\alpha\beta}$ represents the corresponding first-order perturbation of the EM field tensor, V is the effective volume of the cavity, and the angular brackets denote the average values with respect to time. In this case, the displaying condition at the level of a quantum nondemolition measurement can be written as[27]

$$N^{(2)} = \mathscr{E}^{(2)}/\hbar\omega_e \geqslant 1. \tag{13}$$

Then the minimal detectable amplitude of the HFGW, from Eqs. (12) and (13), would be

$$h_{\min} = \frac{1}{2\hat{B}^{(0)}Q}\sqrt{\frac{\mu_0\hbar\omega_e}{V}}, \tag{14}$$

for the non-stochastic HFGW, and

$$h_{\min} = \frac{1}{2\hat{B}^{(0)}}\sqrt{\frac{\mu_0\hbar\omega_e}{QV}}, \tag{15}$$

for the stochastic HFGW.

For the typical parameters of the open superconducting cavity: $V = 0.05$ m^3 ($b = 0.05$ m, $\Delta s = 1$ m^2), $Q = 10^7$, and

using the static magnetic field of $\hat{B}^{(0)} = 9$ T and the resonance condition $\nu_e = \nu_g = 3 \times 10^9$ Hz, one finds (from Eqs. (14) and (15))

$$h_{\min} = 3.9 \times 10^{-23} \quad \text{for the non-stochastic HFGW},$$
$$h_{\min} = 1.2 \times 10^{-19} \quad \text{for the stochastic HFGW}. \tag{16}$$

2.4. Coupling of the planar open cavity with both a static magnetic field and a background EM normal mode

The background EM normal mode in the open cavity can be given by

$$\tilde{E}_x^{(0)} = A^{(0)} \sin\left(\frac{n\pi}{b} z\right) \exp[-\mathrm{i}(\omega_e t + \delta')],$$
$$\tilde{B}_y^{(0)} = -\frac{\mathrm{i}}{\omega_e} \frac{n\pi}{b} A^{(0)} \cos\left(\frac{n\pi}{b} z\right) \exp[-\mathrm{i}(\omega_e t + \delta')], \tag{17}$$

$A^{(0)}$ is the amplitude of the electrical field of the normal mode. Under the resonance condition ($\omega_e = \omega_g$), the first-order perturbation of the energy–momentum tensor produced by the coherent interaction of the perturbative EM normal modes, Eq. (11), with the background normal mode, equation (17) can be written as

$$\langle \overset{(1)}{T}{}_\mu^\nu \rangle_{\omega_e=\omega_g} = \frac{1}{\mu_0} \Big\langle -(F_{\mu\alpha}^{(1)*} F^{\nu\alpha(0)} + F_{\mu\alpha}^{(0)*} F^{\nu\alpha(1)}) + \frac{1}{4} \delta_\mu^\nu (F_{\alpha\beta}^{(1)*} F^{\alpha\beta(0)} + F_{\alpha\beta}^{(0)*} F^{\alpha\beta(1)}) \Big\rangle_{\omega_e=\omega_g}. \tag{18}$$

Then the maximum of the first-order perturbation of energy of the EM field in the cavity (from the 0–0 component of $\overset{(1)}{T}{}_\mu^\nu$ in Eq. (18)) is

$$\mathscr{E}_{\max}^{(1)} = \langle \overset{(1)}{T}{}_0^0 \rangle_{\max} V = \frac{1}{\mu_0 c} A^{(0)} A \hat{B}^{(0)} Q V, \tag{19}$$

where $A = A_\oplus = A_\otimes$ is the amplitude of HFGW. In this case, the maximum of the total signal photon number generated by the first-order perturbation of the EM energy in the cavity will be

$$N_{\max}^{(1)} = \langle \overset{(1)}{T}{}_0^0 \rangle_{\max} V / \hbar\omega_e = \frac{A^{(0)} A \hat{B}^{(0)} Q V}{\mu_0 c \hbar \omega_e}, \tag{20}$$

equations (12), (13), (19), and (20) show that $N_{\max}^{(1)} \gg N^{(2)}$, but $N_{\max}^{(1)}$ is accompanied by large noise photon background caused by the background normal modes, Eq. (17). Thus, the corresponding displaying condition at the level of the background photon noise fluctuation[27,28] is

$$\frac{N_{\max}^{(1)}}{\sqrt{N^{(0)}}} \geqslant 1, \tag{21}$$

where $N^{(0)}$ is the background photon numbers in the cavity. From Eqs. (19)–(21) we have

$$h_{\min} = \frac{1}{\hat{B}^{(0)} Q} \sqrt{\frac{\mu_0 \hbar \omega_e}{V}}, \tag{22}$$

for the non-stochastic HFGW, and

$$h_{\min} = \frac{1}{\hat{B}^{(0)}} \sqrt{\frac{\mu_0 \hbar \omega_e}{QV}} \tag{23}$$

for the stochastic HFGW. Equations (14), (15), and (22), (23) show that in such the two cases (for Subsections 2.1 and 2.2), the minimal detectable amplitudes have the same order of magnitude.

2.5. Coupling of closed cylindrical superconducting cavity with a static magnetic field

For the closed cylindrical cavity having radius R_c and height l, using the similar method in Subsection 2.1 for the open cavity, the fundamental frequency form of the perturbative EM normal model produced by a resonance HFGW can be obtained as (e.g., see Ref. [28]),

$$\tilde{E}_\varphi^{(1)} = A\hat{B}^{(0)} Q c \mathrm{J}_1(k_r r) \cos\left(\frac{\pi}{l} z\right) \exp[\mathrm{i}(-\omega_g t + \delta)],$$
$$\tilde{B}_r^{(1)} = \frac{\mathrm{i} A \hat{B}^{(0)} Q \pi}{k_g l} \mathrm{J}_1(k_r r) \sin\left(\frac{\pi}{l} z\right) \exp[\mathrm{i}(-\omega_g t + \delta)],$$
$$\tilde{B}_z^{(1)} = \frac{\mathrm{i} A \hat{B}^{(0)} Q k_r}{k_g} \mathrm{J}_0(k_r r) \cos\left(\frac{\pi}{l} z\right) \exp[\mathrm{i}(-\omega_g t + \delta)], \tag{24}$$

where

$$k_g^2 = k_r^2 + \left(\frac{\pi}{l}\right)^2, \tag{25}$$

k_r is the radial component of the wave vector, π/l is its longitudinal component, and J_0 and J_1 are the first- and second-rank Bessel functions, respectively, Q is the quality factor of the closed cavity. Then the total perturbative EM energy in the closed cavity is

$$\mathscr{E}^{(2)} = \int \langle \overset{(2)}{T}{}_0^0 \rangle_{\omega_e=\omega_g} \mathrm{d}^3 x' = \frac{1}{\mu_0} (A\hat{B}^{(0)} R_c Q)^2 l \, [\mathrm{J}_0(k_r R_c)]^2. \tag{26}$$

Using the boundary condition $\mathrm{J}_1(k_r R_c) = 0$ at the cavity walls, and considering the typical parameter $\nu_g = 3 \times 10^9$ Hz and Eqs. (24) and (25), we have $k_r R_c = 19.6$, $k_r = 62.7$ m^{-1}, $R_c = 31$ cm, $l = 89$ cm, then $\mathrm{J}_0(k_r R_c) = \mathrm{J}_{0\max}(k_r R_c) = 0.18$. From such parameters, similar to the case of the open cavity (Subsection 2.1), one finds the displaying condition of signal at the level of a quantum nondemolition measurement as follows:

$$N^{(2)} = \mathscr{E}^{(2)} / \hbar\omega_e = \frac{1}{\mu_0 \hbar \omega_e} (A\hat{B}^{(0)} R_c Q)^2 l \, [\mathrm{J}_0(k_r R_c)]^2_{\max} \geqslant 1 \tag{27}$$

and then the minimal detectable amplitude would be

$$h_{\min} = \frac{1}{\hat{B}^{(0)} R_{\rm c} Q \cdot [{\rm J}_0(k_{\rm r} R_{\rm c})]_{\max}} \sqrt{\frac{\mu_0 \hbar \omega_{\rm e}}{l}}, \qquad (28)$$

for the non-stochastic HFGW, and

$$h_{\min} = \frac{1}{\hat{B}^{(0)} R_{\rm c} \cdot [{\rm J}_0(k_{\rm r} R_{\rm c})]_{\max}} \sqrt{\frac{\mu_0 \hbar \omega_{\rm e}}{lQ}}, \qquad (29)$$

for the stochastic HFGW. In general, the quality factor Q of closed superconducting microwave cavities is much higher than that of open superconducting cavities, and under the current technology condition, the Q-value of the closed superconducting cavities can reach up to $Q \sim 10^{11}$ to 10^{12}.[28,29] In this case, for the coupling system of closed cylindrical superconducting cavity ($Q = 10^{11}$, $R_{\rm c} = 0.35$ m, $l = 89$ cm) with the static magnetic field of 9 T, and under the resonance condition $\nu_{\rm e} = \nu_{\rm g} = 3 \times 10^9$ Hz, one finds

$$\begin{aligned} h_{\min} &= 3.0 \times 10^{-26} \quad \text{for the nonstochastic HFGW,} \\ h_{\min} &= 9.3 \times 10^{-21} \quad \text{for the stochastic HFGW.} \end{aligned} \qquad (30)$$

If the background EM fields in the cavity contain both the static magnetic field and an EM normal mode, then the corresponding displaying condition at the level of the background photon noise fluctuation is also the equation (21), but $N^{(1)}_{\max}$ in Eq. (21) should be replaced by the maximum of the first-order perturbative photon number in the closed cylindrical superconducting cavity. Using the same method described in Subsection 2.2, we calculated the minimal detectable amplitude of the HFGW and it is found that such the two cases (the static magnetic field is a unique background EM field or both the static magnetic field and the EM normal mode are presented), the minimal detectable amplitudes have the same order of magnitude. In other words, the presence of the background EM normal modes in the closed cavity does not lead to better sensitivity, i.e., this case is very similar to the open cavity (see Subsection 2.2).

It is necessary to emphasize that the earlier mentioned minimal detectable amplitudes of the resonance cavity systems are not limited sensitivities of superconducting cavities, and these values are only from the above concrete parameters and calculations in this paper. In fact, there is a lot of room to improve their sensitivities due to the following reasons.

a) The quality factors used to the open cavity and the closed cavity in this paper are $Q \sim 10^7$ and $Q \sim 10^{11}$, respectively, while the theoretical limit value of the quality factor for the superconducting microwave cavity might reach up to 10^{16}.[30,31] Moreover, the cavity dimension and the coupling static magnetic field can also be further increased by current technologies. This means that it is still possible to effectively improve the sensitivities of the superconducting cavities, although it will face enormous challenges.

b) If we consider the EM response of the superconducting cavity at a quantum level, e.g., cavity quantum-electrodynamical response to the HFGWs (e.g., see Ref. [32]), one could find a series of novel effects, such as the birefringence effect for the EM normal modes inside cavity, evolution of the quantum states of the EM normal modes, etc., which cannot be found in the framework of pure classical theory. Thus these novel quantum effects might provide new and useful ways to effectively improve the sensitivity.

c) Utilization of squeezed quantum states[5,27,28] for the superconducting resonance cavity could effectively decrease the signal accumulation time for very high quality factor Q (e.g., $Q \sim 10^{12}$ or higher) and improve the sensitivity. In this case, the sensitivity expected theoretically to the superconducting cavity might reach up to $h \sim 10^{-29}$ to 10^{-30}.[5] Consequently, the improved and advanced superconducting cavity systems would be latent and promising schemes of detection for the cosmological HFGWs.

2.6. Synchro-resonance effect in the coupling system of the Gaussian-type microwave photon flux (Gaussian beam (GB)) and the static magnetic field

Unlike the above cases (pure inverse G-effect, the coupling of the inverse G-effect with the coherent plane EM wave, the open cavity and the closed cavity), the signal in the synchro-resonance system (SRS) is the transverse perturbative photon flux (PPF) in the free space, and the PPF (signal photon flux) and the transverse background noise flux (BPF) have very different physical behaviors[22,24,33] in specific local regions, such as different distribution, propagating direction, polarization, decay rate, etc. These different behaviors provide a novel way to distinguish the PPF and the BPF and might reach up a higher sensitivity.

According to the calculation based on electrodynamics and quantum electronics in curved spacetime,[22,24] the transverse first-order PPF (the x direction) can be given by

$$\begin{aligned} n^{(1)}_x &= \frac{c}{\hbar \omega_{\rm e}} \overset{(1)}{\langle T^1_0 \rangle}_{\omega_{\rm e} = \omega_{\rm g}} = \frac{A \hat{B}^{(0)} \psi_0 \Delta l}{4 \mu_0 \hbar \sqrt{1 + (z/f)^2}} \\ &\quad \times \exp\left(- \frac{r^2}{W^2} \right) \cos\left(\frac{k_{\rm g} r^2}{2R} - \tan^{-1} \frac{z}{f} + \delta \right), \end{aligned} \qquad (31)$$

where $\hat{B}^{(0)}$ is the background static magnetic field, ψ_0 is the amplitude of the magnetic field of the GB, Δl is the interaction dimension between the HFGW and the static magnetic field $\hat{B}^{(0)}$, $\overset{(1)}{T^1_0}$ is the 01-component of the first-order perturbation of the energy–momentum tensor of the EM fields in the HFGW, $r^2 = x^2 + y^2$ is the distance to symmetrical axis

of the GB, $k_e = k_g = 2\pi/\lambda_e$ (wave number), $f = \pi W_0^2/\lambda_e$, $W = W_0[1+(z/f)^2]^{1/2}$, W_0 is the minimum spot radius of the GB, $R = z + f^2/z$ is the curvature radius of the wave front of the GB at z, and the z axis is symmetrical axis of the GB.

Thus, the total transverse first-order PPF at an effective receiving surface Δs is

$$\begin{aligned} N_x^{(1)} &= \int_{\Delta s} n_x^{(1)}\,\mathrm{d}y\mathrm{d}z = \frac{A\hat{B}^{(0)}\psi_0\Delta l}{4\mu_0\hbar}\int_{\Delta s}\frac{1}{\sqrt{1+(z/f)^2}} \\ &\quad\times\exp\left(-\frac{r^2}{W^2}\right)\cos\left(\frac{k_g r^2}{2R}-\tan^{-1}\frac{z}{f}+\delta\right)\mathrm{d}y\mathrm{d}z \\ &= \frac{A\hat{B}^{(0)}\psi_0\Delta l}{4\mu_0\hbar}f(k_g,\boldsymbol{x}), \end{aligned} \tag{32}$$

where

$$\begin{aligned} f(k_g,\boldsymbol{x}) &= \int_{\Delta s}\frac{1}{\sqrt{1+(z/f)^2}}\exp\left(-\frac{r^2}{W^2}\right) \\ &\quad\times\cos\left(\frac{k_g r^2}{2R}-\tan^{-1}\frac{z}{f}+\delta\right)\mathrm{d}y\mathrm{d}z \end{aligned} \tag{33}$$

is the matching function (see Fig. 3) between the HFGW and the SRS, which depends on the coupling state between the HFGW and the SRS. Clearly, the maximum $f(k_g,\boldsymbol{x})_{\max}$ of matching functions corresponds to the best coupling.

In this case, the displaying condition of the HFGW in the noise photon flux fluctuation $\sqrt{N^{(0)}_{x(\mathrm{noise})}\Delta t}$ can be given by

$$(N_x^{(1)})^2\Delta t \geqslant N^{(0)}_{x(\mathrm{noise})}, \tag{34}$$

where Δt is the requisite accumulation time of the signal, $N^{(0)}_{x(\mathrm{noise})}$ is the total noise photon flux passing through the effective receiving surface Δs. For the Gaussian-type microwave photon flux, we have[22,23]

$$N^{(0)}_{x(\mathrm{noise})} = (F_{1x}^{(0)} + F_{2x}^{(0)})\exp\left(-\frac{2x^2}{W^2}\right), \tag{35}$$

and $F_{1x}^{(0)}|_{x=0} = 0$, where $F_{1x}^{(0)}\exp(-2x^2/W^2)$ is the transverse background photon flux (BPF) itself of the GB, and $F_{2x}^{(0)}\exp(-2x^2/W^2)$ is the other noise photon flux caused by the BPF. From Eqs. (32)–(35), we obtain

$$h_{\min} = \frac{4\mu_0\hbar}{\hat{B}^{(0)}\psi_0\Delta l\, f_{\max}(k_g,\boldsymbol{x})}\sqrt{\frac{F_{1x}^{(0)}+F_{2x}^{(0)}}{\Delta t}}. \tag{36}$$

Notice that $F_{1x}^{(0)}$ vanishes at the longitudinal symmetrical surface.[34] Thus, the photon fluxes passing through the longitudinal symmetrical surface, will be only $F_{2x}^{(0)}$ (see Eq. (35)), then we have

$$h_{\min} = \frac{4\mu_0\hbar}{\hat{B}^{(0)}\psi_0\Delta l\, f_{\max}(k_g,\boldsymbol{x})}\sqrt{\frac{F_{2x}^{(0)}}{\Delta t}}, \tag{37}$$

where $h_{\min}$ in Eqs. (36) and (37) are the minimal detectable amplitudes of the HFGW at the non-longitudinal symmetrical surface (which is parallel to the longitudinal symmetrical surface) and the longitudinal symmetrical surface, respectively. Equations (36) and (37) show that a key parameter in the SRS is the transverse noise photon flux passing through the effective receiving surface Δs and not, as usually considered as the total noise photon number (or the total noise power). This is because the transverse BPF is a vector and has high directivity. Thus, the sensitivity of the SRS not only depends on the position of the effective receiving surface, but also its space orientation, i.e., the suitable position and the space orientation can provide a better "equivalent antenna gain" and a higher signal-to-noise ratio (SNR) (see Fig. 4). In other words, the larger total noise power in the SRS does not necessarily mean that the photon flux at the effective receiving surface has a lower SNR. Conversely, a smaller total noise power does not necessarily mean that the photon flux at the effective surface has a higher SNR. Only under the condition of the optimal position and best spatial orientation for the effective receiving surface, the photon flux collected at the effective receiving surface will have the best SNR.

For the typical parameters in the SRS: $\hat{B}^{(0)} = 9$ T, $\Delta l = 2$ m, $\psi_0 = 6.5\times10^{-6}$ T (for the GB with $P = 10$ W), $W_0 = 0.06$ m, $y \in [0, 0.05\ \mathrm{m}]$, $z \in [0, 0.3\ \mathrm{m}]$, then equation (36) is reduced to

$$h_{\min} = \frac{4.5\times10^{-36}}{f(k_g,\boldsymbol{x})_{\max}}\sqrt{\frac{F_{1x}^{(0)}+F_{2x}^{(0)}}{\Delta t}}. \tag{38}$$

For the non-stochastic constant amplitude HFGW, $\delta = 11\pi/50$ (or 0.69115) in Eq. (38) is the best phase factor which corresponds the maximum $f(k_g,\boldsymbol{x})_{\max}$ of the matching function (see Fig. 3). For the stochastic HFGW, it is necessary to integrate over all possible phases. Notice that this integration does not equal zero and it is only limited in the positive value region or in the negative value region due to high directivity of the signal photon flux $n_x^{(1)}$ and suitable orientation of the receiving surface. For example, the signal photon flux propagating along the positive direction of the x axis does not provide any contribution for the collected photons at the photon receptor I in Fig. 4, i.e., only the photon flux receptor II can collect this photon flux. Contrarily, the signal photon flux propagating along the negative direction does not provide any contribution for the collected photons at the photon receptor II in Fig. 4, i.e., only the photon flux receptor I can collect this photon flux. Thus a suitable space orientation of the receiving surface locks like a "one-wave valve" with good equivalent antenna gain for the signal photon flux.

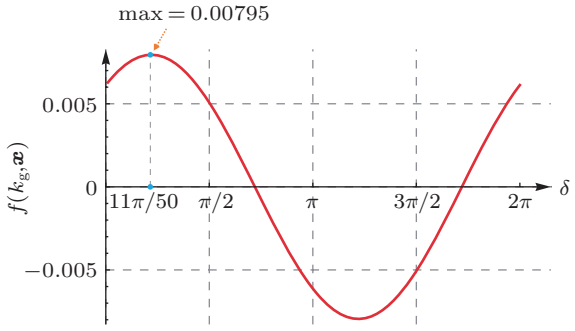


Fig. 3. (color online) Relation curve between the matching function $f(k_g,\boldsymbol{x})$ and the phase δ. δ is the phase difference between the non-stochastic HFGW and the GB in the SRS. It is shown that under the above parameters: $\nu_e = \nu_g = 3\times10^9$ Hz, $W_0 = 0.06$ m, $y \in [0, 0.05$ m$]$, $z \in [0, 0.3$ m$]$, i.e., $\Delta s = 1.5\times10^{-2}$ m^2. For the matching function $f(k_g,\boldsymbol{x})$ at the longitudinal symmetrical surface (i.e., the surface of $x = 0$), then $\delta = 11\pi/50$ (or 0.69115) is the best phase, then $f(k_g,\boldsymbol{x}) = 0.00795$ will be the best matching function.

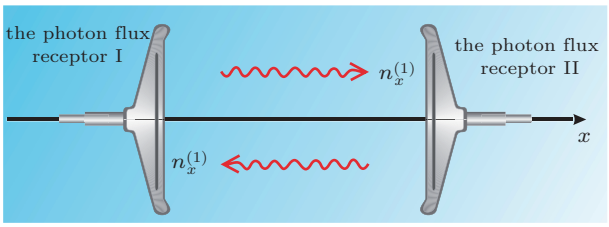


Fig. 4. (color online) Photon receptors I and II to receive photons in different directions. For the $n_x^{(1)}$ propagating along the negative direction of the x axis, only the photon flux receptor I can collect this photon flux. Conversely, only the photon flux receptor II can collect the photon flux $n_x^{(1)}$ propagating along the positive direction of x axis.

According to the above results and calculations, and putting $\Delta t = 10^6$ s in Eq. (37), then even if the peak ($\sim 10^{10}$ s^{-1} for the GB with $P = 10$ W, e.g., see Ref. [24]) of the transverse shot noise photon flux passes the longitudinal symmetrical surface, one finds: $h_{\min} = 5.7\times10^{-32}$ for the non-stochastic constant amplitude HFGW, and $h_{\min} = 1.4\times10^{-31}$ for the stochastic HFGW. However, notably, even for the matching function $f(k_g,\boldsymbol{x})$ not at the longitudinal symmetrical surface (e.g., the surface of $x = 6$ cm, this distance is just one spot radius of the GB), we find $\delta = 3\pi/25$ is the best phase, then $f(k_g,\boldsymbol{x})_{\max} = 0.004989$, i.e., $h_{\min} = 9.1\times10^{-27}$ for the non-stochastic constant amplitude HFGW, and $h_{\min} = 1.4\times10^{-26}$ for the stochastic HFGW. Notice that the BPF $N_x^{(0)}$ at this non-longitudinal symmetrical surface has the maximum $N_x^{(0)} \approx 10^{20}$ s^{-1},[24] and where other noise photon fluxes, such as the diffraction, the reflective noise photon fluxes, etc., are much less than the BPF $N_x^{(0)}$.[33] In other words, then $N_x^{(0)}$ would be the dominate noise source. This means that these results are actually from as such the conservative estimation, and this is satisfactory.

Here, the higher sensitivity in the SRS is mainly from the following facts.

(I) The resonance response of the GB (photon flux) to the HFGW (high-energy gravitons) in the high static magnetic field (virtual photon background) increased effectively their interaction cross section.

(II) Very different physical behaviors (space distribution, propagating direction, decay rate, polarization, etc.)[22–24,33,35] between the signal photon flux and the background photon flux in the local regions of SRS provide a novel effective way to distinguish them.

(III) Enough large EM energy (static and non-static EM energy) contained in the SRS, very low operation temperature ($T \sim 0.14$ K or less), enough long signal integration time ($\sim 10^6$ s or longer), suitable geometric arrangement, and good "antenna gain" of the effective receiving surface, etc; allow the SRS having a sufficiently low standard quantum limit ($\sim 10^{-32}$ to 10^{-34} or less).[36]

Of course, in order to reach up to the above sensitivity, the SRS will face a series of challenges. However, these challenges are from engineering and technology and not a limitation of the basic principle. In other words, they are from the photon-signal-limit, and not the standard quantum limit.[36] Therefore, SRS scheme and its improvement would be always possible.

3. Concluding remarks

I) Frequency bands of the HFGWs expected by the various cosmological models, the brane oscillation scenarios, and the interaction of astrophysical plasma with intense electromagnetic radiation have been extended to the region of $\sim 10^8$ Hz to 10^{12} Hz, which are much higher than the detecting range of the intermediate-frequency detectors (Adv-LIGO, Virgo, GEO, TAMA, etc.) and the low-frequency detectors (LISA, ASTROD, etc.). However, such frequency bands are within the resonance region of the EM detection systems. Thus, the EM detection of such HFGWs would be suitable, and it would be highly complementary to direct observation of GWs in the intermediate-frequency and the low-frequency bands.

II) Best resonance frequency band of the pure inverse G-effect in the typical laboratory dimension would be $\sim 10^8$ Hz to 10^{12} Hz, and the advantage of the inverse G-effect is high sensitivity to the frequency of HFGWs, i.e., the EM signal power flux is proportional to the square ν_g^2 of the HFGW frequency ν_g and it has a good space accumulation effect of the signal in the free space due to the same propagating velocity of both the GWs (gravitons) and the EM waves (photons). However, the signal EM power flux in the inverse G-effect is also proportional to the square A^2 ($A \ll 1$) of the HFGW amplitude A. Because the upper limits of amplitudes for most of

the usual astrophysical and cosmological HFGWs in the microwave band are much less than $\sim 10^{-21}$ to 10^{-24}, thus the HFGWs cannot cause a detectable signal or observable effect in the laboratory condition.

III) Signal EM power fluxes (or signal photon fluxes) in the coupling system of the inverse G-effect with the coherent plane EM wave (background photon flux) include the first-order and the second-order perturbative photon fluxes (PPFs), and maximum of the first-order PPF is much larger than the second-order PPF. However, the presence of the background photon flux (BPF) will generate a large noise photon flux, and because the PPF and the BPF have the same space distribution and propagating direction, then the PPF will be swamped by the noise of BPF. In this case, the sensitivity in the coupling system may be improved by one to two orders of magnitude, but cannot be improved much beyond the pure inverse G-effect. Nevertheless, a coupling system between the higher static magnetic field and the coherent EM wave would be a better detection scheme, this is because increasing strength of the static magnetic field does not increase the number of the background real photon (noise). Notice that under the present technology condition, the strength of the static magnetic field can be already ~ 40 T or larger. In this case, the detection of the HFGWs in the brane oscillation models and in some high-energy astrophysical process may be promising in the future.

IV) Advantages of the superconducting detection cavities include very high quality factor Q (the perturbative EM fields in the cavities are proportional to the quality factor Q), the suitable size (it is often smaller than that of the inverse G-effect) and high sensitivity to the HFGWs in the microwave band. However, the perturbative EM energies (signal) in the detection cavities are almost independent of the frequencies of the HFGW in the resonance frequency bands, and only depends on the amplitudes of the HFGWs. In other words, a major contribution of the HFGWs to the perturbative EM energies in the coupling cavities are from their amplitudes but not frequencies.

Nevertheless, a very high limit value of the quality factor ($Q \sim 10^{16}$) and novel quantum effects of the EM normal modes in the superconducting cavity, will provide a large improvement to the sensitivity. Therefore, improved and advanced superconducting cavity schemes will be promising for detection of the cosmological HFGWs.

V) Advantages of the SRS are from the sensitivity to the frequencies as well as the energy densities of HFGWs (i.e., very high frequency would compensate for weak HFGW amplitude), very different physical behaviors between the signal photon flux and the background photon flux in the local regions, and very low standard quantum limit. However, the SRS will face a series of technological challenges, such as the detection of a weak photon flux, construction of a high and compact static magnetic field, the generation and tuning of a Gaussian-type microwave photon flux with high-quality and very low operation temperature and hard vacuum environment, etc. Nevertheless, these challenges and difficulties are from engineering and technology and not basic principles. Thus, there still is a broad room for improvement for the SRS. If we consider an optimal coupling system between the SRS and the superconducting cavity, then the sensitivity would be effectively improved due to advantages of both the SRS and the superconducting resonance cavity. Such schemes, and related issues will be considered elsewhere.

References

[1] Cuadrado G G 2009 *AIP Conf. Proc.* **1103** 553
[2] Tong M L and Zhang Y 2009 *Phys. Rev. D* **80** 084022
[3] Giovannini M 1999 *Phys. Rev. D* **60** 123511
[4] Giovannini M 2009 *Class. Quantum Grav.* **26** 045004
[5] Bisnovatyi-Kogun G S and Rudenko V R 2004 *Class. Quantum Grav.* **21** 3347
[6] Cruise A M 2012 *Class. Quantum Grav.* **29** 095003
[7] Press W H and Thorne K S 1972 *Ann. Rev. Astron. Astrophys.* **10** 335
[8] Abbott B P, *et al*. 2009 *Nature* (London) **460** 990
[9] Gasperini M and Veneziano G 2003 *Phys. Rep.* **373** 1
[10] Veneziano G 2004 *Sci. Am.* **290** 54
[11] Clarkson C and Seahra S S 2007 *Class. Quantum Grav.* **24** F33
[12] Servin M and Brodin G 2003 *Phys. Rev. D* **68** 044017
[13] Sivaram C and Arun K 2011 arXiv: 0708.3343 [astro-ph]
[14] Chen P 1994 Stanford Linear Accelerator Center Report (SLAC-PUB-6666) March 23, 1994, Rome, Italy, p. 379
[15] Wu X G and Fang Z Y 2008 *Phys. Rev. D* **78** 094002
[16] Li F Y and Tang M X 2002 *Int. J. Mod. Phys. D* **11** 1049
[17] Nikishov A I and Ritus V I 1990 *Sov. Phys. JETP* **71** 643
[18] Chen P 1991 *Mod. Phys. Lett. A* **6** 1069
[19] Gertsenshtein M E 1962 *Sov. Phys. JETP* **14** 84
[20] Boccaletti D, De Sabbata V, Fortint P and Gualdi C 1970 *Nuovo Cim. B* **70** 129
[21] De Logi W K and Mickelson A R 1977 *Phys. Rev. D* **16** 2915
[22] Li F Y, Tang M X and Shi D P 2003 *Phys. Rev. D* **67** 104008
[23] Li F Y, Yang N, Fang Z Y, Baker R M L Jr, Stephenson G and Wen H 2009 *Phys. Rev. D* **80** 064013, arXiv: 0909.4118v2 [gr-qc]
[24] Li J, Lin K, Li F Y and Zhong Y H 2011 *Gen. Relativ. Gravit.* **43** 2209
[25] Li F Y and Baker R M L Jr 2007 *Int. J. Mod. Phys. B* **21** 3274
[26] Li F Y, Chen Y and Wang P 2007 *Chin. Phys. Lett.* **24** 3328
[27] Grishchuk L P and Sazin M V 1983 *Sov. Phys. JETP* **53** 1128
[28] Grishchuk L P 2003 arXiv: gr-qc/0306013
[29] Bessonov E G 1998 arXiv: physics/9802037 [physics.class-ph]
[30] Braginsky V B, Caves C M and Thorne K S 1977 *Phys. Rev. D* **15** 2047
[31] Braginsky V B and Khalili F Y 1999 *Phys. Lett. A* **257** 241
[32] Gerlach U H 1992 *Phys. Rev. D* **46** 1239
[33] Woods R, Baker R M L Jr, Li F Y, Stephenson G V, Davis E W and Beckwith A W 2011 *J. Mod. Phys.* **2** 498
[34] Yariv A 1989 *Quantum Electronics*, 3rd edn. (New York: Wiley)
[35] Li J, Li F Y and Zhong Y H 2009 *Chin. Phys. B* **18** 922
[36] Stephenson G V 2009 *AIP Conf. Proc.* **1103** 542